Highly Tunable Syngas Product Ratios Enabled by Novel Nanoscale Hybrid Electrolytes Designed for Combined CO_2 Capture and Electrochemical Conversion

Tony G. Feric[a,c], Sara T. Hamilton[b,c], Byung Hee Ko[d], Ga-Hyun Annie Lee[a,c], Sumit Verma[e], Feng Jiao[d] and Ah-Hyung Alissa Park[a,b,c,*]

[a]Department of Chemical Engineering, Columbia University, New York, NY 10027, USA

[b]Department of Earth and Environmental Engineering, Columbia University, New York, NY 10027, USA

[c]Lenfest Center for Sustainable Energy, Columbia University, New York, NY 10027, USA

[d]Department of Chemical Engineering, University of Delaware, Newark, DE 19716, USA

[e]Shell International Exploration and Production Inc., Houston, TX 77082, USA

Corresponding author: ap2622@columbia.edu

Keywords

CO_2 capture and conversion, Electrolyte, CO_2 reduction, CO_2RR, Nanoparticle Organic Hybrid Materials (NOHMs), Polymers, Nanoparticles, Electrochemistry

Abstract

This is the author manuscript accepted for publication and has undergone full peer review but has not been through the copyediting, typesetting, pagination and proofreading process, which may lead to differences between this version and the Version of Record. Please cite this article as doi: 10.1002/adfm.202210017.

Coupling renewable energy with the electrochemical conversion of CO_2 to chemicals and fuels has been proposed as a strategy to achieve a new circular carbon economy and help mitigate the effects of anthropogenic CO_2 emissions. Liquid-like Nanoparticle Organic Hybrid Materials (NOHMs) are composed of polymers tethered to nanoparticles and were previously explored as CO_2 capture materials and electrolyte additives. In this study, two types of aqueous NOHM-based electrolytes were prepared to explore the effect of CO_2 binding energy (*i.e.,* chemisorption vs. physisorption) on CO_2 electroreduction over a silver nanoparticle catalyst for syngas production. Poly(ethylenimine) (PEI) and Jeffamine M2070 (HPE) were ionically tethered to SiO_2 nanoparticles to form the amine-containing NOHM-I-PEI and ether-containing NOHM-I-HPE, respectively. At less negative cathode potentials, PEI and NOHM-I-PEI-based electrolytes produced CO at higher rates than 0.1 molal. $KHCO_3$ due to favorable catalyst-electrolyte interactions. Whereas at more negative potentials, H_2 production was favored because of the carbamate electrochemical inactivity. Conversely, HPE and NOHM-I-HPE-based electrolytes displayed poor CO_2 reduction performance at less negative potentials. At more negative potentials, their performance approached that of 0.1 molal. $KHCO_3$, highlighting how the polymer functional groups of NOHMs can be strategically selected to produce value-added products from CO_2 with highly tunable compositions.

1. Introduction

Though renewable energy technologies have advanced rapidly over the last couple of decades, integration with the grid is currently challenged by intermittency and storage issues.[1–3] Thus, the design and development of technologies which can directly convert and store excess renewable energy on the large scale could help mitigate the effects of climate change.[3–6] For example, the renewables-powered electrochemical conversion of CO_2 to chemicals and fuels is an attractive means of avoiding and/or reducing CO_2 emissions, while creating a new circular carbon economy. When considering liquid solvent systems designed only for CO_2 capture, the solvent regeneration step is energy intensive, especially for aqueous systems where the heat capacity of water is very large (4.18 kJ kg^{-1} K^{-1}).[7] Thus, it is proposed to drive the capture of CO_2 with subsequent electrochemical conversion, which is known to be a promising route to upgrade CO_2 to a variety of C_1 and C_2 compounds. The renewables-powered electrochemical CO_2 conversion would be a transformative pathway for closing the carbon cycle.

The electrochemical production of syngas, or a mixture of H_2 and CO, has been proposed for several applications and they require specific H_2 to CO ratios. Examples include

methanol synthesis (H_2/CO ratio of 2), dimethyl ether formation (H_2/CO ratio of 1), syngas fermentation (H_2/CO ratio ranging from 1 to 3.33) and Fischer-Tropsch reactions (H_2/CO ratio of 2).[8–11] The direct electrochemical production of some compounds is not currently possible with high selectivity and reactivity, thus the formation of syngas could be a useful first step to avoid costly downstream separations.[8–11] Evidently, the optimal ratios of H_2/CO are quite different depending on the application of the syngas so the development of electrochemical systems which could produce a wide range of syngas compositions would be especially useful. An alternative approach would be to develop a system where a CO producing unit exists separately from a H_2 producing electrolyzer, so that they can be independently optimized. Several advances have been made in terms of catalyst[5,12–14] and reactor[5,14–16] design for the electrochemical conversion of CO_2, though aqueous CO_2 electroreduction is also limited due to the low solubility of CO_2 in the electrolyte phase.[5,17,18] Thus, the development of innovative electrolytes with improved CO_2 solubilities has been proposed to improve the performance of the CO_2 electroreduction reaction (CO_2RR) and other electrochemical reactions relevant to energy storage applications, such as flow batteries.[17–24]

The effects of incorporating ionic liquids,[19,20,25,26] small ligands,[27] surfactants,[28,29] deep eutectic solvents[30–33] and/or amines[28,33–36] to electrolytes for the CO_2RR have recently been studied. In addition to improving the CO_2 solubility of the electrolytes, in some cases, these additives behaved as co-catalysts for the CO_2RR as a reduction in overpotential, tuned product selectivity and/or improved reaction rates were observed. Ionic liquids are promising candidates because they have been widely shown to significantly enhance the performance of the CO_2RR.[37–41] Furthermore, a careful analysis of experimental and computational data has revealed that the ionic liquid plays a crucial role in stabilizing CO_2RR intermediates at the catalyst surface.[19,20,40,42–44] As a result, electrolytes with an optimal CO_2 binding energy that can enhance the performance of the CO_2RR are highly sought after because an integration of CO_2 capture with the CO_2RR can remove the need for the energy intensive CO_2 capture solvent regeneration.[24,35]

Nanoparticle Organic Hybrid Materials (NOHMs) consist of an organic polymer tethered to an inorganic nanoparticle core via either covalent or ionic bond.[45–48] Owing to their favorable properties, including negligible vapor pressure,[46] oxidative-thermal stability,[46,49–51] chemical tunability[52,53] and high conductivity,[54,55] NOHMs have been extensively studied for CO_2 capture[45,49,50,52,55–61] and several electrochemical applications.[53,62–66] Because of the myriad of possible nanoparticle and polymer combinations, NOHMs are a highly versatile class of materials that can be designed for targeted applications. For electrochemical energy storage applications in particular, developing an understanding the structural and transport properties of innovative electrolyte materials has been shown to be essential to improving the overall system performance.[67–72]

Though NOHMs have shown to possess great properties for CO_2 capture, their application in the neat state is typically limited by a reduced polymer mobility and an order of magnitude larger viscosity when compared to the untethered polymers.[46,73–75] By mixing NOHMs with a secondary fluid, such as water, it was found that the viscosity dropped significantly.[46] Thus, we have recently investigated the effect of the secondary fluid properties,[74] ionic stimulus,[71,75] NOHMs concentration[71] and bond type[48] on the resulting transport behaviors and structure of the polymer canopy in NOHMs. The results of these studies have shown that the polymer canopy in NOHMs composed with an ionic bond, in particular, are highly responsive to the chemical environment (*i.e.,* solvent quality, ionic stimulus and/or NOHMs concentration)[71,74,75] making NOHMs promising candidates to study as electrolyte additives for a variety of energy storage processes. Because of their ability to increase the concentration of CO_2 in aqueous electrolytes, NOHMs have been proposed for combined CO_2 capture and conversion applications,[62,76] though their exact role

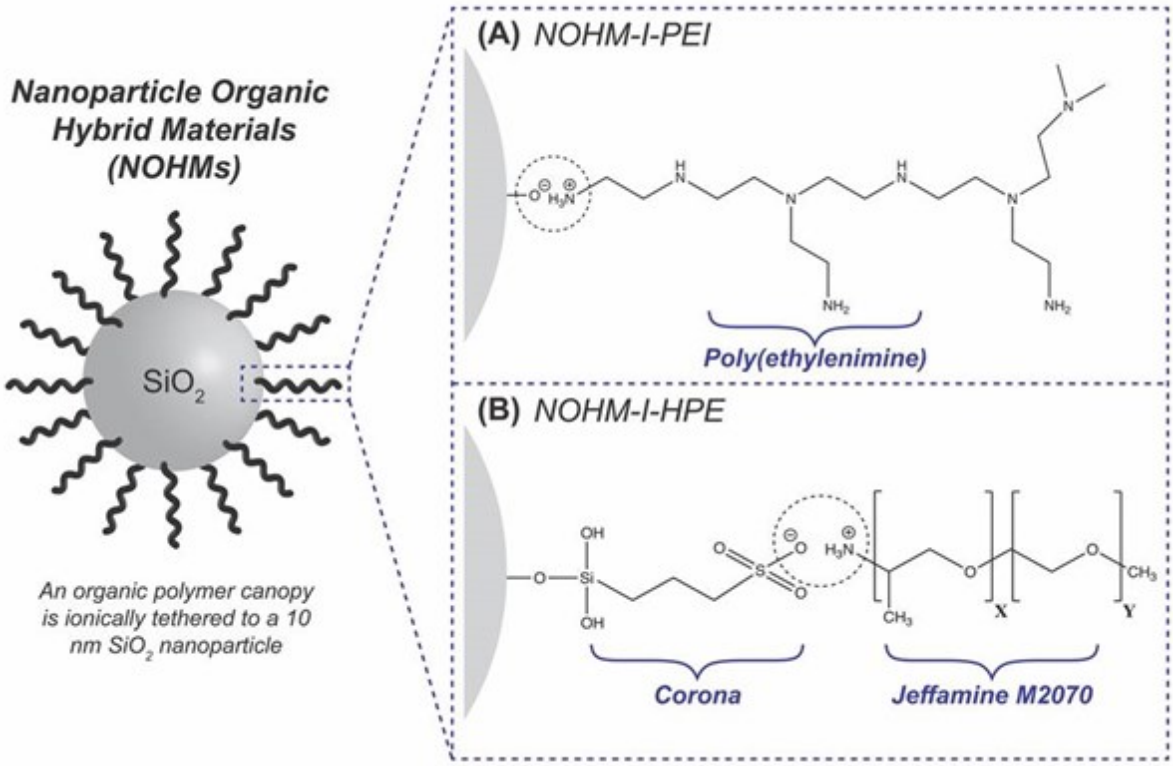

Figure 1. Schematic of **(A)** NOHM-I-PEI and **(B)** NOHM-I-HPE. The X and Y in the Jeffamine M2070 (HPE) canopy represent the number of poly(propyleneoxide) groups (10)

in the CO_2 conversion process has not been reported on. For this first in-depth study of NOHM-mediated CO_2 capture and conversion, a silver nanoparticle catalyst was selected because of its well-known ability to produce CO and H_2 at different ratios, depending on the applied potential.

In this study, we prepared two different types of NOHMs to explore the effect of polymer functional groups in the NOHMs canopy on the resulting CO_2 capture and conversion behaviors over a silver nanoparticle catalyst. We synthesized the amine containing NOHM-I-PEI and the ether containing NOHM-I-HPE by ionically tethering branched poly(ethylenimine) (PEI) and Jeffamine M2070 (HPE), respectively, to ~10 nm SiO_2 particles. The structures of the resulting materials are shown in **Figure 1A** and **1B,** respectively. Additionally, we measured the CO_2 capture capacities of various polymer and NOHM-based fluids/electrolytes across a range of CO_2 partial pressures (P_{CO2} = 0.04 – 1 atm). Finally, we tested the CO_2RR performance of the CO_2 saturated untethered polymer and NOHM-based electrolytes on a silver nanoparticle catalyst at potentials ranging from -0.6 to -1.2 V vs. RHE, and compared their performance to that of CO_2 saturated 0.1 molal. $KHCO_3$. The results from this study elucidate that NOHMs can be used as materials enabling combined CO_2 capture and conversion, and provide a unique reaction environment for the electrochemical reduction of CO_2.

2. Results and Discussion

2.1 CO_2 capture behaviors of PEI and NOHM-I-PEI solutions as a function of CO_2 partial pressure

Compared to non-aqueous solvents, water is a significantly cheaper and safer, and thus, widely used for many electrochemical applications.[17] Unfortunately, its CO_2 solubility is limited to about 34 mM, or 0.034 mmol CO_2/g.[5,17,18] As a result, when developing novel electrolytes for the integrated capture and conversion of CO_2, it will be necessary to determine the electrolyte CO_2 concentration at a wide range of CO_2 capture conditions and address any potential challenges associated with limited CO_2 solubility. In this study, we investigated the CO_2 capture kinetics and capacities of 8 wt.% PEI and 10 wt.% NOHM-I-PEI aqueous solutions at CO_2 partial pressures ranging from 0.04 to 1 atm. The total amount of CO_2 captured was expected to increase with the polymer/NOHMs concentration due to the increased amount of CO_2 binding functional groups in the solution. However, in our recently published studies, we found that the viscosity of untethered polymers around 2000 MW and the corresponding NOHMs began to increase rapidly above a concentration of 10 wt.%.[74,75] Thus, here we employed a concentration of 10 wt.% NOHM-I-PEI to maximize the CO_2 loading in the electrolyte while minimizing mass transfer limitations. Since the NOHM-I-PEI is composed of roughly 20 wt.% SiO_2, an 8 wt.% solution of PEI would contain the same amount of polymer in solution as 10 wt.% NOHM-I-PEI, and was used as a comparison for all CO_2 capture and CO_2 reduction experiments in this study. Moreover, the concentrations of

CO_2 were selected to represent industrial exhaust gases from gas turbines (4% CO_2), coal-fired power plants (10-15% CO_2) and cement manufacturing (14-33% CO_2).[77,78] Concentrations of 65% CO_2 and 100% CO_2 were selected to further understand the CO_2 capture performance across a broad concentration range.

The CO_2 capture of amine-containing solutions has been well-studied throughout the literature.[79–83] For every mole of amine, primary (R_1NH_2) and secondary amines (R_1R_2NH) are known to capture 0.5 moles of CO_2. The overall reaction can be represented by

$$CO_2 + 2R_1R_2NH \rightleftharpoons R_1R_2NCOO^- + R_1R_2N^+H_2 \quad \textbf{Eq. (1)}$$

though there has been some debate about the exact reaction mechanism. The two main mechanistic pathways which have been presented in the literature are the two-step zwitterion mechanism[79–82] and the single-step termolecular mechanism.[83] According to the zwitterion mechanism, the reaction of CO_2 with a primary or secondary amine results in the formation of a zwitterion which is then deprotonated by another amine (Eq. 4) or water molecule (Eq. 5).[79–82] The zwitterion mechanism can be represented by the following

$$CO_2 + R_1R_2NH \rightleftharpoons R_1R_2N^+HCOO^- \quad \textbf{Eq. (2)}$$

$$R_1R_2N^+HCOO^- + R_1R_2NH \rightleftharpoons R_1R_2NCOO^- + R_1R_2N^+H_2 \quad \textbf{Eq. (3)}$$

$$R_1R_2N^+HCOO^- + H_2O \rightleftharpoons HCO_3^- + R_1R_2N^+H_2 \quad \textbf{Eq. (4)}$$

Conversely, Da Silva and Svendsen claimed that the zwitterion is not stable enough to be reliably detected and the reaction takes place in a single step whereby the CO_2 reacts with the base and the proton transfer to the water or amine molecule occurs at the same time.[83] More recent reports on mechanistic pathways of CO_2 capture by primary and/or secondary amines provide evidence for the zwitterion mechanism, as reaction intermediates have been clearly identified with spectroscopic tools.[79–82]

Because they lack protons, the zwitterion formed upon reaction of tertiary amines ($R_1R_2R_3N$) with CO_2 can only be deprotonated by water molecules. Thus, the mechanism by

which tertiary amines react with CO_2 is generally known to occur by the following reaction steps

$$CO_2 + R_1R_2R_3N \rightleftharpoons R_1R_2R_3N^+COO^- \quad \textbf{Eq. (5)}$$

$$R_1R_2R_3N^+COO^- + H_2O \rightleftharpoons HCO_3^- + R_1R_2R_3N^+H \quad \textbf{Eq. (6)}$$

The overall reaction mechanism can be represented by

$$CO_2 + R_1R_2R_3N + H_2O \rightleftharpoons HCO_3^- + R_1R_2R_3N^+H \quad \textbf{Eq. (7)}$$

whereby the theoretical uptake of 1 mole CO_2 per mole of amine can be achieved. It should be noted that because the irreversible formation of the charged carbamate species during the reaction of CO_2 with amines in solution leads to significantly improved conductivities,[28,84] CO_2-loaded amine suspensions have recently been explored for CO_2 conversion applications.[28,33–36,85]

The kinetic CO_2 uptake of 8 wt.% PEI and 10 wt.% NOHM-I-PEI solutions is presented in **Figure 2A** and **2B**, respectively. As expected, the CO_2 capture rate and capacity increased with the CO_2 partial pressure. Additionally, polymer tethering in NOHM-I-PEI does not appear to have a significant impact on the total CO_2 capture capacity suggesting that all amine groups in NOHMs are available to capture CO_2. Our prior studies have shown that NOHMs composed of an ionic bond display enhanced oxidative-thermal stability compared to the untethered polymer,[45,46,49,51] thus suggesting that NOHMs can serve as robust materials for applications involving harsh reaction conditions.

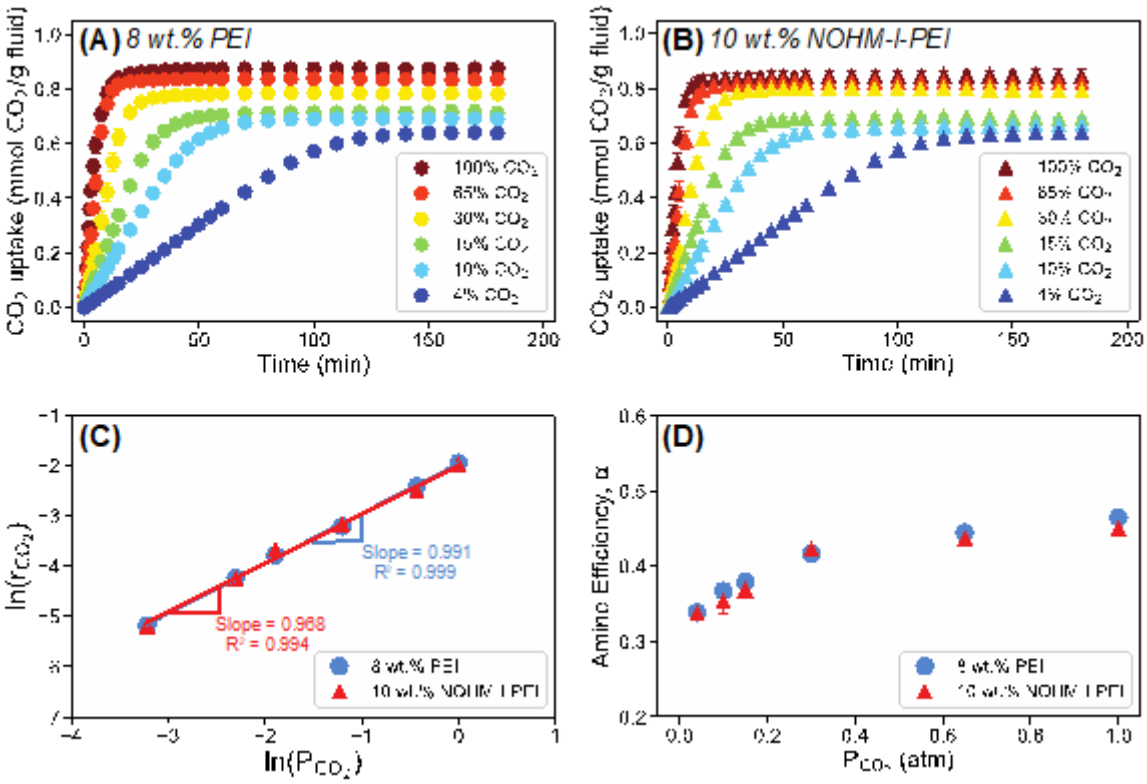

Figure 2. Kinetic CO_2 uptake of **(A)** 8 wt.% PEI and **(B)** 10 wt.% NOHM-I-PEI solutions measured at P_{CO2} = 0.04 to 1 atm. **(C)** Determination of the order of the reaction for CO_2 capture in 8 wt.% PEI and 10 wt.% NOHM-I-PEI. **(D)** Amine efficiency plotted as a function

The order of the reaction with respect to CO_2 was determined by the slope of the logarithm of the initial rate of CO_2 capture against the logarithm of the CO_2 partial pressure (See **Figure 2C**). It is apparent that the PEI and NOHM-I-PEI curves are overlapping which suggests that polymer tethering also does not pose constraints on the rate of CO_2 capture in NOHM-I-PEI. Additionally, the order of the reaction with respect to CO_2 was observed to be 1 in the case of 8 wt.% PEI and 10 wt.% NOHM-I-PEI, as has been reported for other amine-containing solutions.[79] This signifies that the relationship between the CO_2 capture rate and the CO_2 partial pressure is linear, which could be an important design parameter when developing integrated CO_2 capture and conversion processes.

To understand how effectively the amine groups in the PEI are capturing CO_2 in the aqueous solutions of PEI and NOHM-I-PEI, the dimensionless amine efficiency was employed. The amine efficiency, α, describes the ratio of moles of CO_2 captured to the moles of amines in the solution and can be calculated by

$$\alpha = \frac{mol\ CO_2\ captured}{mol\ N\ in\ solution} \quad \textbf{Eq. (8)}$$

Knowing the CO_2 capture capacity and the number of amines (~47 moles of amine per mole of PEI), the amine efficiency was calculated and plotted as function of the CO_2 partial pressure in **Figure 2D** for 8 wt.% PEI and 10 wt.% NOHM-I-PEI. As has been reported for similar aqueous suspensions of amines, the amine efficiency increased with CO_2 partial pressure and approached a value of about 0.5 at P_{CO2} = 1 atm, the theoretical maximum for primary and secondary amines in aqueous solution.

2.2 Determining the optimal $KHCO_3$ concentration for CO_2RR in the presence of polymer and NOHM additives

While PEI and NOHM-I-PEI solutions are ionically conductive, they are not as conductive as the conventional electrolytes. Thus, supporting electrolyte (*i.e.,* 0.1 molal. $KHCO_3$) was added to further improve the ionic conductivity of aqueous NOHM-based solutions and enhances their functionality for electrochemical applications. We studied the effect of $KHCO_3$ concentration on the CO_2 capture capacity and initial CO_2 capture rate of the aqueous suspensions of PEI and NOHM-I-PEI, at a partial pressure of P_{CO2} = 0.15 atm, which is representative of CO_2 concentrations in flue gases.[77,78] **Figure 3A** and **3B** depict the kinetic CO_2 uptake data for 8 wt.% PEI and 10 wt.% NOHM-I-PEI, respectively, as the salt concentration was increased from 0.0 molal. to 1.0 molal $KHCO_3$. An initial inspection of the data revealed that the initial rate of CO_2 capture did not change as the salt concentration increased, though the CO_2 capture capacity (per g of fluid) steadily decreased with salt addition. By plotting the initial rate of CO_2 capture and the amine efficiency (α) as a function of the salt concentration in **Figure 3C** and **3D**, respectively, these trends can be more directly observed. The fact that the initial rate of CO_2 capture remained unaffected by the salt concentration is an excellent finding which suggests that the salt ions (i.e., K^+, HCO_3^- and/or CO_3^{-2}) do not impede the ability of the amine functional groups of the PEI polymer to capture CO_2.

Moreover, the reduced CO_2 capture capacity of the electrolytes as the salt is added can be explained by a combination of solution pH and CO_2 equilibrium effects. Since, CO_2 is a weakly acidic gas, a higher pH value (*i.e.,* more basic solution) will ensure a higher driving energy for CO_2 capture.[85] **Figure 3D** also displays the measured pH values of 8 wt.% PEI and 10 wt.% NOHM-I-PEI electrolytes as a function of $KHCO_3$ concentration, and as salt

was added, the pH steadily declined. Additionally, the HCO_3^- anion is known to partition between the CO_3^{-2} and CO_2 species in aqueous solutions as shown in the following equilibrium reactions

$$CO_2 + H_2O \rightleftharpoons H_2CO_3 \quad \textbf{Eq. (9)}$$

$$H_2CO_3 \rightleftharpoons H^+ + HCO_3^- \quad \textbf{Eq. (10)}$$

$$HCO_3^- \rightleftharpoons H^+ + CO_3^{-2} \quad \textbf{Eq. (11)}$$

Thus, the addition of a significant amount of $KHCO_3$ in the solutions could introduce more CO_3^{-2} and HCO_3^- species initially, which would then limit additional CO_2 loading in the amine solutions.

Because there was almost no difference between the total CO_2 capture capacity when there was no salt and 0.1 molal. $KHCO_3$ loaded into the electrolytes, this salt concentration was selected for CO_2RR experiments over the silver nanoparticle catalyst. Similar concentrations of $KHCO_3$ have been reported for use in the CO_2RR throughout the literature because of the ability of the bicarbonate ion to serve as an excellent buffer[17,86,87] and increase local concentrations of CO_2 near the electrochemical interface.[88] In a similar fashion, we also confirmed that the addition of 0.1 molal. $KHCO_3$ did not reduce the CO_2

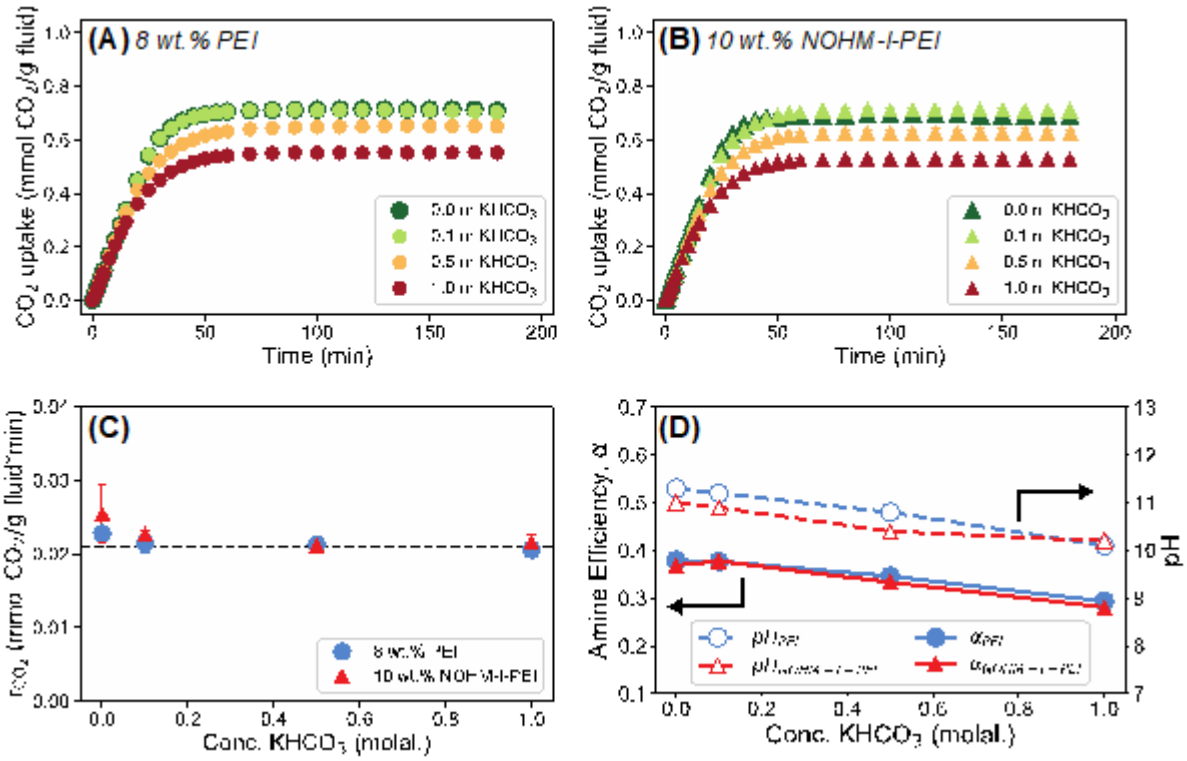

Figure 3. Effect of $KHCO_3$ concentration on the CO_2 capture behaviors of **(A)** 8 wt.% PEI and **(B)** 10 wt.% NOHM-I-PEI, at P_{CO2} = 0.15 atm. **(C)** Initial CO_2 uptake rate and **(D)** amine efficiency and pH plotted as a function of the $KHCO_3$ concentration for 8 wt.% PEI and 10 capture capacity (P_{CO2} = 1 atm) of the 8 wt.% HPE and 10 wt.% NOHM-I-HPE solutions as well (See **Figure S1**).

2.3 Impact of polymer functional groups on CO_2 capture capacity and electrolyte pH and conductivity

The goal of this study was to employ NOHMs of variable CO_2 binding energy (*i.e.,* chemisorption vs. physisorption) to understand the resulting effect on the CO_2RR. Thus, we

synthesized NOHMs composed of polymers with ether groups (*i.e.,* NOHM-I-HPE) and amine groups (*i.e.,* NOHM-I-PEI) ionically tethered to SiO_2 nanoparticles. It is widely known that aqueous amine solutions capture CO_2 via chemisorption and ether groups interact with CO_2 via physisorption. **Figure 4** presents the CO_2 capture capacity of the 8 wt.% PEI, 10 wt.% NOHM-I-PEI, 8 wt.% HPE, 10 wt.% NOHM-I-HPE and an aqueous solution of 0.1 molal. $KHCO_3$, at P_{CO2} = 1.0 atm. It is clear that the addition of any of the polymers or NOHMs studied led to an increase in the CO_2 capture capacity. Additionally, it was found that the amine containing polymers/NOHMs had about an order of magnitude higher CO_2 capture capacity than their ether containing counterparts.

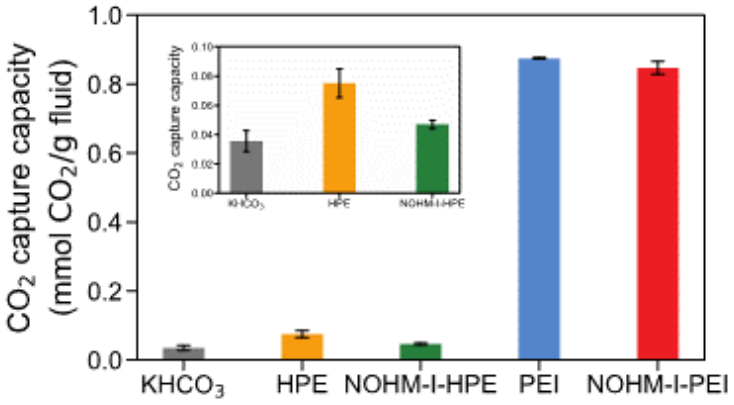

Figure 4. CO_2 capture capacity represented for 0.1 molal. $KHCO_3$, 8 wt.% HPE, 10 wt.% NOHM-I-HPE, 8 wt.% PEI and 10 wt.% NOHM-I-PEI at 25°C and P_{CO2} = 1 atm. Polymer and NOHM-based fluids were not doped with any

As mentioned previously, the concentrations of polymers and NOHMs tested were strategically selected to normalize for the mass of inert SiO_2 present in the NOHMs samples. Thus, it was expected for the CO_2 capture capacity to be very similar between the corresponding untethered polymer and NOHM-based solutions. However, the 8 wt.% HPE displayed a CO_2 capture capacity which was notably higher than that of the 10 wt.% NOHM-I-HPE. This can be explained by the presence of free -NH_2 groups in the untethered Jeffamine M2070 polymer (See **Figure 1B** for the structure of HPE), which would be expected to capture some CO_2 via chemisorption. More specifically, in the HPE chain, there is about 1 amine group per polymer chain, which has about 41 repeat units. In NOHM-I-HPE, the amine terminus is used as the site of ionic tethering to the SiO_2 nanoparticle, and thus would not be expected to participate in CO_2 capture in the same manner as a primary amine. Similarly, NOHM-I-PEI was observed to have a slightly lower CO_2 capture capacity than the corresponding PEI solution, though the difference much less significant due to the larger number of amine groups present in the polymer backbone.

The electrolyte pH[89–91] and conductivity[32,87] have also been shown to influence product selectivity and formation rates in electrochemical CO_2 reduction. Thus, we measured the pH and conductivity of 0.1 molal. $KHCO_3$ and the 4 polymer/NOHMs solutions mentioned above doped with 0.1 molal. $KHCO_3$, after being purged with N_2 and CO_2 for 30 min. The results are displayed in **Figure 5**. When purged with N_2, the pH of all of the

solutions were variable and ranged from 8.7 to 10.8, due to the different functional groups present. Conversely, upon CO_2 capture, the solutions all displayed a pH very close to 7. As the pH of the electrolyte has been shown to affect the CO_2RR performance,[89–91] it is important that the bulk pH is well controlled and accounted for in CO_2RR experiments. Since this was the case, no further pH control technique was applied to the CO_2-purged electrolytes employed in this study.

The conductivity of the 0.1 molal. $KHCO_3$ (6.12 ± 0.31 mS/cm), 8 wt.% PEI (5.64 ± 0.28 mS/cm) and 10 wt.% NOHM-I-PEI (5.22 ± 0.26 mS/cm) purged with N_2 were quite similar. PEI is reportedly known to possess a conductive nature due to the large number of amine groups, some of which can become protonated when dissolved in water.[53] Thus, it was not expected to see a significant drop in the conductivity of the PEI and NOHM-I-PEI based electrolytes compared to the 0.1 molal. $KHCO_3$. Contrarily, the conductivity of the 8 wt.% HPE (4.05 ± 0.20 mS/cm) and 10 wt.% NOHM-I-HPE electrolytes (3.63 ± 0.18 mS/cm) were notably lower than that of the 0.1 molal. $KHCO_3$, suggesting that the ether groups along the HPE backbone do not contribute to solution conductivity and the addition of bulky polymer components reduced the overall mobility of ions in solution. Upon CO_2 exposure for 30 min, the conductivity of 0.1 molal. $KHCO_3$ (6.08 ± 0.30 mS/cm), 8 wt.% HPE (4.43 ± 0.22 mS/cm) and 10 wt.% NOHM-I-HPE (3.77 ± 0.19 mS/cm) remained relatively unchanged. As mentioned previously, the reaction of CO_2 with amines in aqueous suspensions leads to the formation of charged carbamate species[28] (See Equation 3), and thus, the conductivity of 8 wt.% PEI (8.85 ± 0.44 mS/cm) and 10 wt.% NOHM-I-PEI (8.56 ± 0.43 mS/cm) increased by a factor of about 1.5. It should be noted that the conductivity of the NOHMs were slightly lower than that of the corresponding untethered polymer.

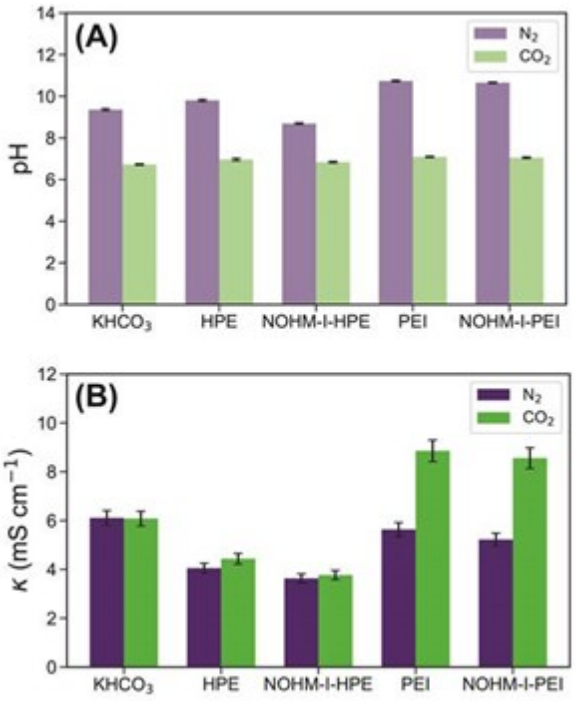

Figure 5. Measured **(A)** pH and **(B)** ionic conductivity of 0.1 molal. $KHCO_3$, 8 wt.% HPE, 10 wt.% NOHM-I-HPE, 8 wt.% PEI and 10 wt.% NOHM-I-PEI after being purged with N_2 or CO_2 for 30 min. All polymer and NOHMs samples

Overall, the change in functional groups in the polymer canopy of NOHMs will ultimately affect the electrolyte CO_2 capture capacity, pH and conductivity. Ideally,

electrolytes with high CO_2 capture capacity and conductivity are desired for CO_2RR applications. However, it was important to understand whether the captured CO_2 in NOHM-based electrolytes is electrochemically active.

2.4 Effect of varying CO_2 binding energy of NOHMs on CO_2 electrochemical conversion over a silver nanoparticle catalyst

After demonstrating the improved CO_2 capture capacity of the NOHM-I-PEI and NOHM-I-HPE electrolytes compared to one of the conventional CO_2RR electrolytes (*i.e.,* 0.1 molal. $KHCO_3$), we explored the effect of the NOHMs on the CO_2RR by performing 1-hr chronoamperometry experiments over a silver nanoparticle catalyst, in an H-cell. The gas-phase products of the aqueous CO_2RR, namely H_2 and CO, were measured throughout the course of the reaction and the Faradaic efficiency (FE) of the reactions is depicted in **Figure 6** for the 5 electrolytes employed in this study. Additionally, the measured current density responses are reported in **Figure S2** as a function of time. **Figure 6A** shows the gas-phase product distribution for the electrolysis of a CO_2 purged 0.1 molal. $KHCO_3$ solution. As is typically observed for silver catalysts, the CO selectivity increased significantly as the

applied cathode potential became more negative.[28,29,92,93] It should be noted that the H_2 and CO faradaic efficiencies and current densities observed in this study for 0.1 molal $KHCO_3$ at -1.0 V vs. RHE were in agreement with the literature for silver catalysts employed for the CO_2RR, thus ensuring our confidence in the results (See Table S1).

Upon inspection of the data presented in **Figure 6B** and **6C**, the selectivity of the CO_2RR was clearly distinct when the electrolyte was changed to 8 wt.% PEI or 10 wt.% NOHM-I-PEI. For example, at less negative potentials (*i.e.,* -0.6 and -0.7 V vs. RHE) the

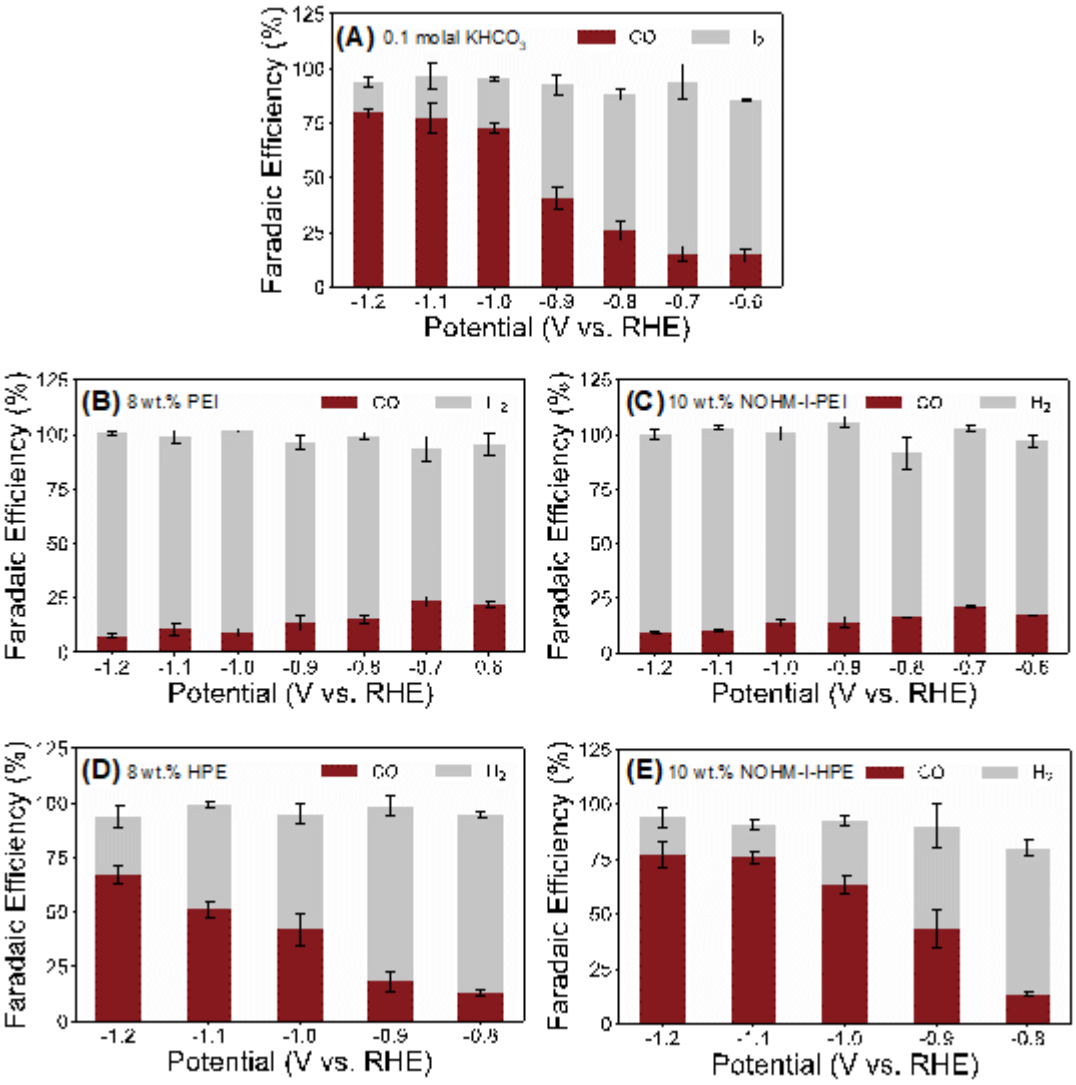

Figure 6. Faradaic efficiency distribution of the 1 hr chronoamperometry of CO_2 purged (**A**) 0.1 molal. $KHCO_3$, (**B**) 8 wt.% PEI, (**C**) 10 wt.% NOHM-I-PEI, (**D**) 8 wt.% HPE and (**E**) 10 wt.% NOHM-I-HPE over a silver nanoparticle catalyst. All polymer and NOHMs samples were doped with 0.1 molal. $KHCO_3$ and 3 experimental trials were conducted at each iR-

FE_{CO} was about 5% higher when compared to the FE_{CO} of CO_2RR in 0.1 molal. $KHCO_3$. This observation suggests that the conversion of "free" CO_2 at low applied potentials was facilitated in the presence of the absorbed PEI or NOHM-I-PEI layer on the surface of the electrode. CO_2 confined in that electrolyte layer seemed to have different electrochemical reaction behaviors and our future studies will further probe this effect. On the other hand, as the potential became more negative, the FE_{CO} slightly decreased in 8 wt.% PEI or 10 wt.% NOHM-I-PEI-based electrolytes, suggesting that catalyst-electrolyte interactions and/or the strength of the carbamate bond limit the ability of captured CO_2 to be converted electrochemically. Thus, while a strong CO_2 binding energy (e.g., carbamate bonds) is favored in terms of achieving a high CO_2 loading in the electrolyte, it challenges the conversion of captured CO_2 unless energy is added to release CO_2 into an electrochemically active form (e.g., a thermal swing similar to the solvent regeneration step used for CO_2 capture technologies).

Conversely, the electrolytes containing HPE and NOHM-I-HPE displayed a much more similar FE distribution of the H_2 and CO to the 0.1 molal. $KHCO_3$ case (See **Figure 6D** and **6E**), especially at more negative applied potentials (*i.e.,* -1.0, -1.1 and -1.2 V vs. RHE). At less negative potentials, such as -0.8 and -0.9 V vs. RHE, the H_2 evolution reaction (HER) was observed to dominate in HPE and NOHM-I-HPE containing electrolytes. These results demonstrate that the chemistry of the polymer canopy and the resulting binding energy for CO_2 can be used to tune the selectivity of the NOHM-mediated CO_2RR.

Furthermore, in the case of PEI and NOHM-I-PEI-based electrolytes, polymer tethering did not appear to significantly change the distribution of the product formation as the FE for H_2 and CO remained more or less equivalent across the potential range. However, the FE_{CO} was 10-15% higher for NOHM-I-HPE-based electrolytes when compared to the untethered HPE-based electrolytes. In our recent mechanistic study of NOHM-mediated Zn electrodeposition, we showed that the polymer tethering in NOHM-I-HPE led to noticeable differences in the electrochemical deposition of Zn over a glassy carbon electrode, when compared to the untethered HPE. Briefly, the HPE canopy organization around the bulky SiO_2 nanoparticle was demonstrated to affect the delivery of Zn^{+2} ions to the electrode surface, as evidenced by enhancements in the overall current density of the deposition reaction and the exchange current density after Zn deposition.[66] The adsorbed layer of NOHMs on the electrode surface led to multiple transport pathways. Based on the improvement of FE_{CO} in the NOHM-I-HPE compared to the untethered HPE in this study, a slight benefit of the polymer structure in the NOHM-I-HPE was also observed. Taken together, the findings presented in this study, therefore, suggest that the polymer functional groups and their structure/conformation may also play a significant role at the electrochemical interface, in particular for heterogenous reactions such as the CO_2RR.

The results presented in **Figure 6** illustrate that the NOHMs play a role in tuning the products of CO_2RR, however, they do not give any indication of the effect of NOHMs on the

rate of CO_2 conversion. Thus, the partial current density of H_2 (j_{H2}) and CO (j_{CO}) formation at a given potential were determined by multiplying the calculated FE (See **Figure 6**) by the respective total steady state current density (j_{tot}) of the CO_2RR (See **Figure S2**). For example, the following can be used to determine j_{H2} and j_{CO}, respectively

$$j_{H_2} = j_{tot} \times FE_{H_2} \quad \textbf{Eq. (12)}$$

$$j_{CO} = j_{tot} \times FE_{CO} \quad \textbf{Eq. (13)}$$

Using Equation 12 and 13, the partial current densities of H_2 and CO were calculated and plotted in **Figure 7** as a function of the applied potential for the 5 electrolytes explored in this study. It should be noted that the total current density of CO_2RR produced by electrolytes containing HPE and NOHM-I-HPE was notably lower than the other electrolytes studied (See **Figure S2**). It is suggested that strong catalyst-electrolyte interactions between the HPE canopy and the electrode limited the overall current density, since the applied potentials for all bulk electrolysis experiments were iR-corrected. Thus, using the same experimental conditions (*i.e.,* electrode area and CO_2 sweep gas flowrate), accurate product detection was not possible at -0.6 and -0.7 V vs. RHE for these HPE and NOHM-I-HPE-based electrolytes.

In **Figure 7A**, it is evident that the HPE-based electrolyte displayed a similar amount of H_2 production compared to 0.1 molal. $KHCO_3$ in the entire potential range tested, while the 10 wt.% NOHM-I-HPE-based electrolyte displayed a slight suppression in the rate of H_2 formation, which is highly desired for CO_2RR applications. However, the rate of CO production in the HPE and NOHM-I-HPE electrolytes was slightly reduced compared to that of the 0.1 molal. $KHCO_3$, likely due to strong interactions between the HPE and the electrode surface blocking some of the catalytic active sites. The overall potential dependent CO_2RR performance of electrolytes containing HPE and NOHM-I-HPE matched the trends observed in the 0.1 molal. $KHCO_3$. For example, the rate of H_2 formation remained relatively constant at potentials more negative than -0.8 V vs. RHE while the rates of CO production continually increased as more negative potentials were applied (See **Figure 7B**).

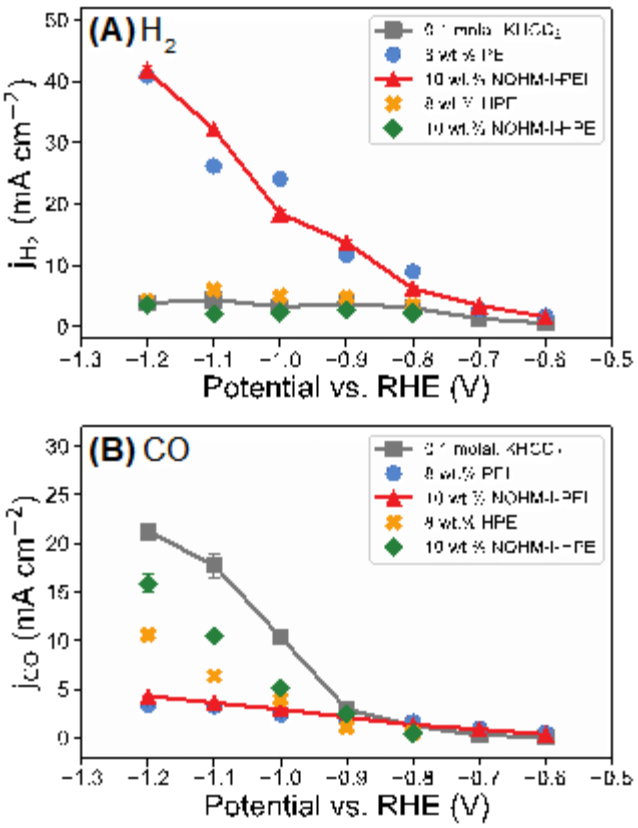

Figure 7. Partial current density of **(A)** H_2 and **(B)** CO formation represented as a function of the iR-corrected potential for CO_2 purged 0.1 molal. $KHCO_3$, 8 wt.% PEI, 10 wt.% NOHM-I-PEI, 8 wt.% HPE and 10 wt.% NOHM-I-HPE, during 1 hr chronoamperometry over a silver nanoparticle catalyst. All polymer and NOHMs samples were

Moreover, the PEI and NOHM-I-PEI-based electrolytes displayed opposing H_2 and CO production trends compared to those described for 0.1 molal. $KHCO_3$. In particular, the rates of H_2 production continually increased as more negative potentials were applied, whereas the CO production appeared to plateau as the potential reached -1.2 V vs. RHE. These findings revealed that at less negative applied potentials, favorable interactions between the amine functional groups of the PEI and NOHM-I-PEI-based electrolytes could promote the electrochemical conversion of "free" CO_2. Conversely, at more negative potentials, the room

temperature electrochemical stability of the carbamate bond[35,36,94] and/or unique catalyst-electrolyte interactions led to a favoring of the HER, over a silver nanoparticle catalyst. These observations are in good agreement with recent literature reports documenting the CO_2 reduction behaviors of aqueous amine-electrolytes under similar reaction conditions (See Table S2).

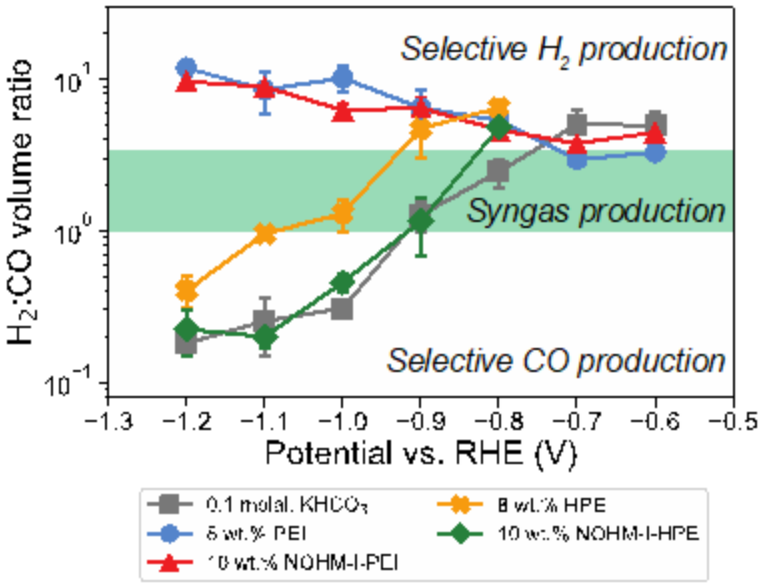

Figure 8. Effect of iR-corrected potential on the H_2:CO product ratio for CO_2 purged 0.1 molal. $KHCO_3$, 8 wt.% PEI, 10 wt.% NOHM-I-PEI, 8 wt.% HPE and 10 wt.% NOHM-I-HPE, during 1 hr chronoamperometry over a silver nanoparticle catalyst. All polymer and NOHMs samples were doped with 0.1 molal. $KHCO_3$ and 2 experimental trials were

Because the formation of some compounds via CO_2RR is currently limited by low selectivity and reaction rate (*i.e.,* methanol synthesis), the production of tunable syngas ratios via electrochemical pathways can be an invaluable tool for the development of chemical precursors for a variety of processes.[8,9] The syngas ratios (H_2/CO) for the aqueous CO_2RR of a silver nanoparticle catalyst in the 5 electrolytes explored in this study are reported in **Figure 8** as a function of the applied potential and **Figure 9** illustrates the effect of the polymer canopy's CO_2 binding energy on the observed CO_2RR behaviors in NOHM-based electrolytes. Overall, the polymer and NOHM-based electrolytes were able to form syngas at H_2/CO ratios ranging from 0.22 ± 0.08 (NOHM-I-HPE at -1.2 V vs. RHE) to 11.85 ± 1.24 (NOHM-I-PEI at -1.2 V vs. RHE), highlighting their ability to be used in applications with varying H_2 and CO concentration requirements, such as, methanol synthesis (H_2/CO ratio of 2), dimethyl ether formation (H_2/CO ratio of 1), syngas fermentation (H_2/CO ratio ranging from 1 to 3.33) and Fischer-Tropsch reactions (H_2/CO ratio of 2).[8–11] It is important to note that the addition of NOHMs to the electrolyte was observed to reduce the current density of CO_2RR at most applied potentials, when compared to the 0.1 molal. $KHCO_3$. However, the results of this study have informed the design of NOHMs which can facilitate the efficient delivery of CO_2 to the electrode surface for conversion to upgraded chemicals and fuels. For example, conductive polymers with an intermediate CO_2 binding energy and a stimuli responsive (e.g., magnetic field, light, pH, salt concentration etc.) nanoparticle are desired to enable the facile reaction of CO_2 at the electrode interface and tune the composition of the electrolyte double layer, respectively.

Furthermore, CO_2 bound strongly to NOHMs containing amine moieties could be promoted for electrochemical reduction through a moderate thermal swing process (e.g., temperature of

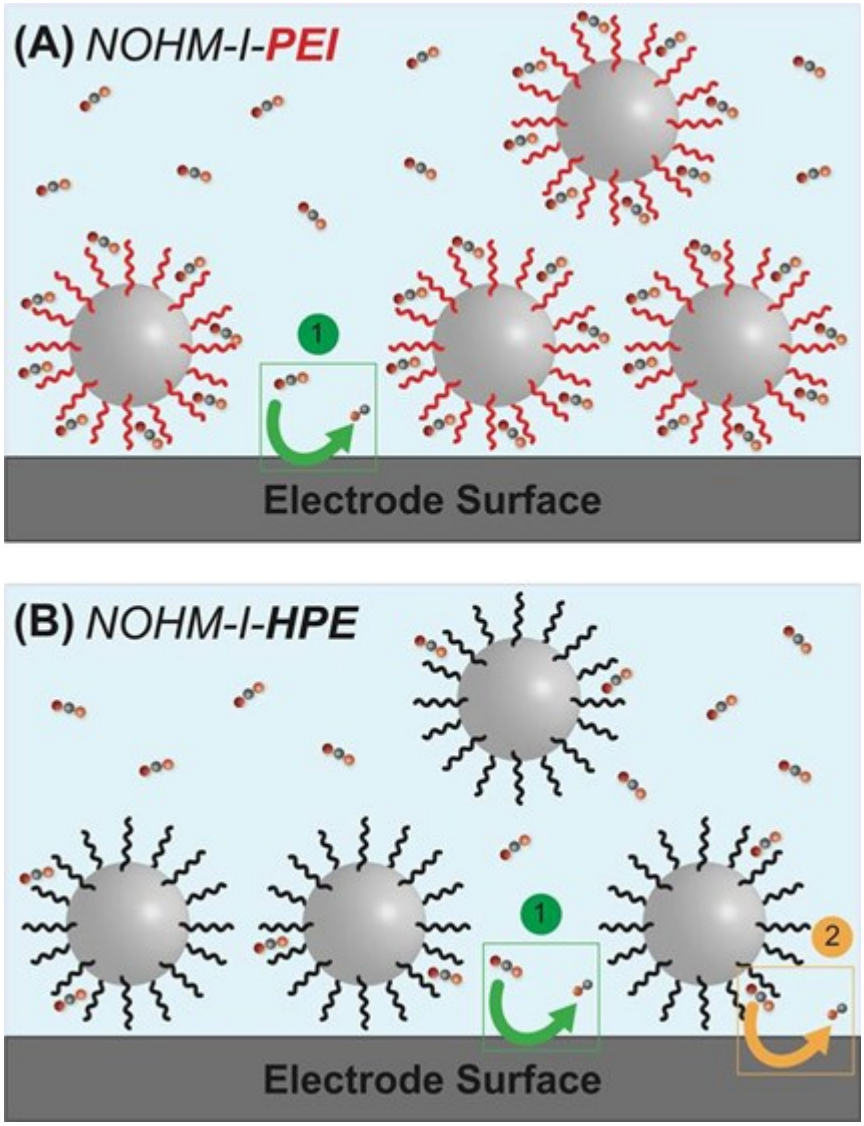

Figure 9. Schematic representing the different proposed CO_2 reduction pathways in NOHM-based electrolytes. (A) When the binding energy between the functional groups in the polymer canopy of NOHMs is too strong and results in carbamate formation, only "free" CO_2 can be converted under ambient temperature, as depicted by Pathway 1. (B) When the CO_2 is captured by NOHMs via physisorption, the weakly bound CO_2 can be converted (e.g., Pathway 2) in

60-75 °C), as has recently been demonstrated.[35,36] This energy transfer could be efficiently applied through careful selection of the nanoparticle core. Both electrolyte and reactor/process design will be critical to effectively combine CO_2 capture with conversion at industrially relevant rates.

2.5 Exploring catalyst-NOHMs interactions via SEM-EDS imaging

It was hypothesized that strong catalyst-polymer interactions led to the observed differences in the product distributions and current densities associated with the iR-corrected CO_2 electrolysis when PEI, NOHM-I-PEI, HPE or NOHM-I-HPE were introduced to the electrolyte, compared to the 0.1 molal. $KHCO_3$. Throughout the literature, probing the catalyst-electrolyte interactions has been demonstrated to be insightful in further understanding the effect of novel electrolytes in CO_2 conversion.[19,20,30,40,42–44] As a result, we employed a scanning electron microscope (SEM) coupled with energy dispersive X-ray

spectroscopy (EDS) analysis to detect the presence of polymers and NOHMs on the silver nanoparticle electrode surface after CO_2 conversion.

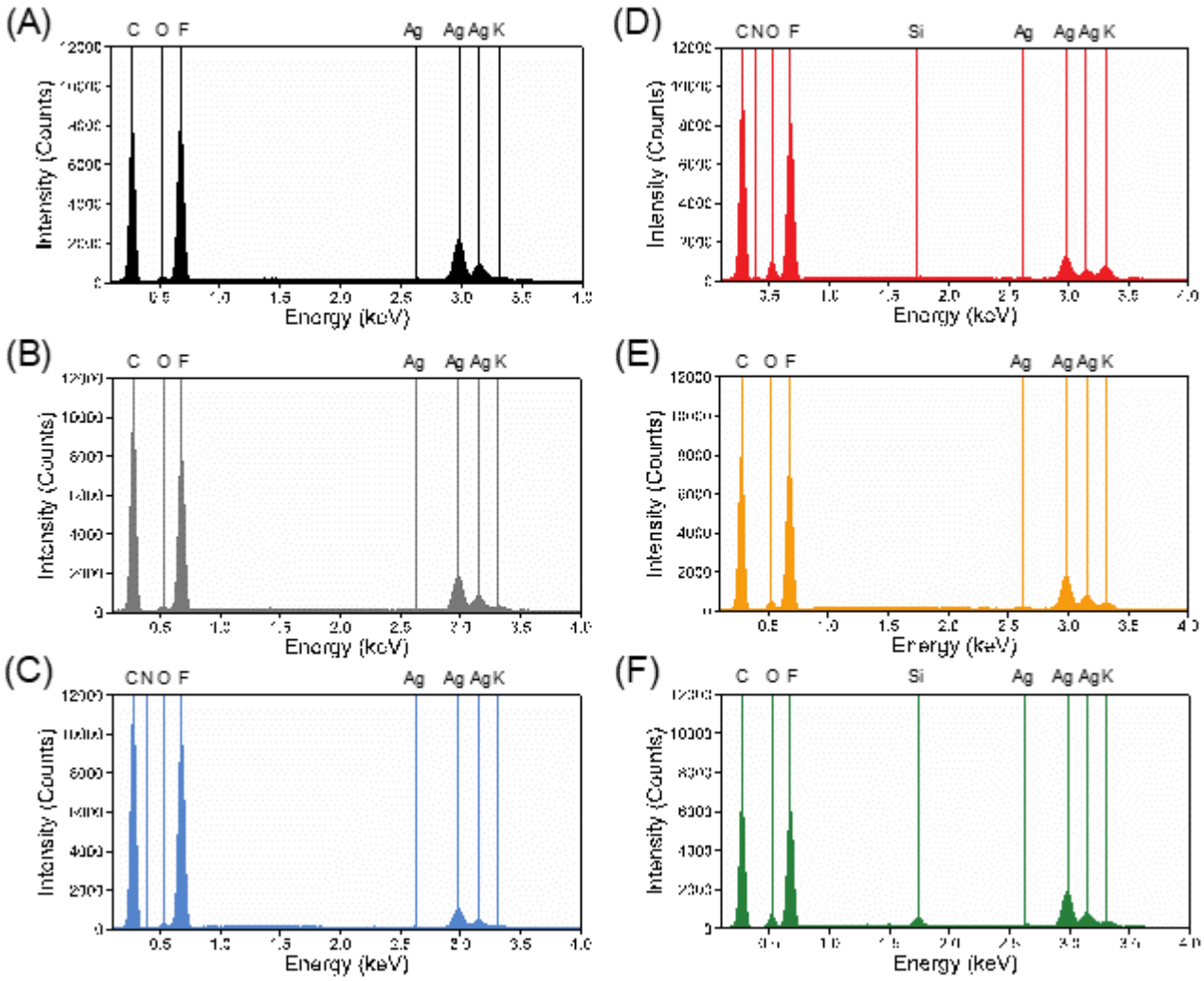

Figure 10. EDX identification of the elements present on the **(A)** neat Ag nanoparticle surface and after 1-hr of CO_2 electrolysis at -1.2 V vs. RHE in **(B)** 0.1 molal. $KHCO_3$, **(C)** 8 wt.% PEI, **(D)** 10 wt.% NOHM-I-PEI, **(E)** 8 wt.% HPE and **(F)** 10 wt.% NOHM-I-HPE. The electrolytes containing

The SEM images of the neat electrode and after 1-hr electrolysis in the 5 electrolytes tested in this work are shown in **Figure S3**, **S4** and **S5**, at three different magnification levels. After CO_2RR was completed, the electrodes were rinsed and then dried overnight with a vacuum oven. Then, an EDS technique was applied to map the elemental composition of the electrode surface with the aim of detecting species unique to the polymer and NOHM-based electrolytes (*i.e.,* N and/or Si). The elemental mapping obtained from the EDS analysis is shown in **Figure 10** and the results clearly depict the detection of N on the electrodes which had CO_2RR performed in 8 wt.% PEI and 10 wt.% NOHM-I-PEI, as expected. Additionally, the electrodes which were employed for CO_2 reduction in 10 wt.% NOHM-I-PEI and 10

wt.% NOHM-I-HPE displayed the presence of Si peaks, demonstrating the surface adsorption of NOHMs. It should be noted that the N and Si peaks detected are quite small, but the electrodes were analyzed applying a rinsing procedure, which suggests that the polymer and/or NOHMs detected on the surface of the electrode are quite strongly adsorbed during the CO_2RR. Overall, these findings revealed that the polymers and NOHMs employed in this study have unique interactions with the Ag nanoparticle catalyst, though more in-depth electrode surface characterization tools are required to probe the exact nature of the catalyst-electrolyte interactions. The results of this study illustrate that not only is it important to improve the solubility of CO_2 in the electrolyte, but the catalyst-electrolyte interactions need to promote the subsequent conversion of the captured CO_2. By probing the nature of the electrochemical interface during the CO_2RR, polymer canopies with optimized functional groups (*i.e.,* CO_2 binding energy, conductivity, pH, viscosity) can be identified for enhanced CO_2 conversion performance.

3. Conclusions

In this study, we observed that the NOHM-mediated electrochemical conversion of CO_2 on a silver nanoparticle catalyst led to a change in the selectivity and reaction rate of the product formation when compared to the conventional aqueous electrolyte (*i.e.,* 0.1 molal. $KHCO_3$). In particular, we explored the effect of the polymer functional groups of NOHMs on the electrochemical conversion of CO_2. For example, the CO_2-loaded PEI and NOHM-I-PEI containing electrolytes displayed increased total reaction rates at all applied potentials. At -0.8 V vs. RHE, the PEI and NOHM-I-PEI containing electrolytes were found to produce CO at a slightly higher rate (1.65 ± 0.03 mA cm^{-2}, 1.33 ± 0.01 mA cm^{-2}) than the 0.1 molal. $KHCO_3$ (1.26 ± 0.05 mA cm^{-2}). Alternatively, at -1.2 V vs. RHE, the CO formation reached a plateau for PEI and NOHM-I-PEI containing electrolytes (3.41 ± 0.03 mA cm^{-2}, 4.32 ± 0.03 mA cm^{-2}) while the CO formation significantly increased as the applied potential became more negative for 0.1 molal. $KHCO_3$ (21.21 ± 0.47 mA cm^{-2}). This was explained to be a result of the inability of the carbamate bond to be broken electrochemically at 25 °C[35,36,94] and unique interactions between the functional groups of the PEI polymer and the surface of the electrode promoting the HER. Furthermore, at all applied potentials the total current density was slightly lower for HPE and NOHM-I-HPE electrolytes compared to the 0.1 molal. $KHCO_3$. At -0.8 V vs. RHE, CO formation rates in the HPE and NOHM-I-HPE electrolytes were noticeably lower (0.53 ± 0.01 mA cm^{-2}, 0.45 ± 0.01 mA cm^{-2}), while at -1.2 V vs. RHE their performance approached that of the 0.1 molal. $KHCO_3$ (10.63 ± 0.41 mA cm^{-2}, 15.89 ± 0.93 mA cm^{-2}). Under most of the conditions explored, the NOHM-based electrolytes performed as well as or better than the corresponding untethered polymer-based electrolytes. Additionally, liquid-like NOHMs composed of an ionic bond have been shown

to display a higher oxidative-thermal stability than the corresponding untethered polymers,[45,49,51,74] thus illustrating their robustness as functional materials under harsh oxidizing conditions. Moreover, the multitude of polymer, linker and nanoparticle combinations will allow for the design of materials that are responsive to a change in the environment (*i.e.,* temperature, pH, ionic stimulus and/or magnetic field) that can be used in a variety of integrated CO_2 capture and conversion applications. Overall, the results of this work demonstrated that NOHMs appear to be promising electrolyte additives for combined CO_2 capture and conversion applications, and the further design of NOHM-based electrolyte should focus on more conductive polymer canopies with intermediate CO_2 binding energy and NOHMs with functionalized cores.

4. Experimental Section

4.1 Synthesis of NOHM-I-PEI. Liquid-like NOHM-I-PEI was synthesized as previously reported and a representative structure is shown in Figure 1A.[45,52,53] Briefly, a 3 wt.% mixture of 10 nm diameter SiO_2 nanoparticles (Ludox SM-30, obtained from Sigma Aldrich) in deionized water was prepared and then stirred for at least 30 minutes. To replace any positively charged cations with protons, the diluted silica suspension was then run through a cation exchange column filled with 50 g of Dowex Marathon C hydrogen form (Sigma Aldrich). Next, the silica nanoparticles were functionalized by the dropwise addition of a 20 wt.% solution of branched poly(ethylenimine) (MW = 2000 g/mol, Polysciences Inc.) in deionized water, while stirring. According to the manufacturer, the poly(ethylenimine) (referred to as PEI) contains primary, secondary and tertiary amines at an approximate ratio of 40/36/24. Once all of the PEI had been added to the nanoparticles, the solution was then left to stir for several hours. Then, this solution was placed in a vacuum oven set to ~60 °C overnight to evaporate the excess water. In this study, the mass ratio of PEI to SiO_2 is roughly 80:20 in the resulting NOHM-I-PEI. Before preparing any samples, neat PEI and NOHM-I-PEI were placed in the vacuum oven at 75 °C for two hours to ensure the removal of any absorbed moisture and/or CO_2.

4.2 Synthesis of NOHM-I-HPE. Liquid-like NOHM-I-HPE was synthesized using previously described methods and a representative structure is shown in **Figure 1B**.[46,51,57–59,74,95–97] 18.3 g of a 30 wt.% colloidal suspension of 10 nm diameter SiO_2 nanoparticles (Ludox SM-30 obtained from Sigma-Aldrich) was diluted to a concentration of 4 wt.% in deionized water. 30 g of a 35 wt.% 3-(trihydroxysilyl)-1-propane-sulfonic acid solution (Gelest Inc.) was further diluted to a final concentration of 7 wt.%. The silica suspension was then added to the silane solution in a dropwise manner. Then, 1 M NaOH was added dropwise to this solution to a pH of 5 and the final solution was stirred at 70 °C for 24 hrs.

Excess silane linker molecules were removed by dialyzing the solution against deionized water for a total of 48 hrs (SnakeSkin Dialysis Tubing 3500 MW cutoff, Thermo Scientific) with frequent water changing. To protonate the sulfonate groups on the linker molecules and remove any other cations, the surface functionalized silica nanoparticles were then passed through a cation-exchange resin (Dowex Marathon C hydrogen form, Sigma Aldrich).

Next, an amine-terminated polyether, Jeffamine M2070 (MW=2000 g/mol, acquired from Huntsman Co.), was ionically tethered to the functionalized nanoparticles. A 20 wt.% solution of Jeffamine M2070 (referred to as HPE) in deionized water was titrated into the functionalized silica nanoparticles solution until the equivalence point was reached (pH = 6.5), where all the linker groups were neutralized. The resulting solution containing the ionically tethered polymers was placed in a vacuum oven at 60 °C for 24 hrs to remove the water used in the previous steps. Prior to performing any experiments, neat HPE and NOHM-I-HPE were placed in a vacuum oven at 75 °C for at least 2 hrs, in order to remove any absorbed moisture.

4.3 Gravimetric measurement of CO_2 capture capacity. The CO_2 capture capacity of various polymer and NOHM-based fluids/electrolytes were measured gravimetrically. Gas tanks containing different mixtures of CO_2 and N_2 were used to simulate flue gases with different partial pressures of CO_2 ranging from 0.04 to 1 atm. About 20 g of the polymer or NOHM-based fluid/electrolyte was loaded into a 3-neck valve fitted with a 2 μm gas sparger (Fisher) on one of the ports. The two remaining ports were fitted with small outlet vents to prevent pressure buildup within the cell. The CO_2 containing gas stream was continuously fed at 100 mlpm to the port fitted with the gas sparger after first passing through a bubbler to minimize solvent evaporation. During the course of the reaction, the 3-neck cell was weighed at several time points using an analytical balance (AB104-S/FACT, Mettler Toledo, precision of 10^{-4} g) and the increase in mass was converted to absorbed moles of CO_2 (MW =44.01 g/mol). The reaction was performed at room temperature, ~ 25 °C.

4.4 pH and ionic conductivity measurement. The pH and ionic conductivities of the 0.1 molal. $KHCO_3$, 8 wt.% PEI, 10 wt.% NOHM-I-PEI, 8 wt.% HPE and 10 wt.% NOHM-I-HPE were measured after being purged with N_2 or CO_2 for 30 minutes. It should be noted that all polymer and NOHM-based electrolytes were doped with 0.1 molal. $KHCO_3$. The pH of these electrolytes was measured at room temperature using a previously calibrated benchtop pH meter (Fisher Scientific). The ionic conductivities of these electrolytes were measured at 25 ± 1 °C using an S230 SevenCompact benchtop conductivity meter (Mettler Toledo) equipped with a micro 2 platinum poles conductivity probe (Cond probe InLab 752 – 6mm, Mettler Toledo), which can measure conductivities in the range of 0.01 – 112 mS cm^{-1}. The uncertainty in conductivity was determined to be within ± 5% for all samples.

4.5 Ag nanoparticle electrode preparation. The electrodes employed in this study were prepared using a previously reported method.[98] Briefly, the catalyst ink was prepared

by mixing 100 mg Ag nanoparticles (<100 nm, 99.5%, Sigma-Aldrich) and 10 wt.% (metal basis) Nafion ionomer (5 wt.% in 50/50 water and isopropanol, Fuel Cell Store) in 10 mL deionized water and 10 mL isopropanol. After sonicating for 1 h, the catalyst ink was air-sprayed onto Sigracet 39 BB gas diffusion layer (Ion Power) at 100 ℃ until ~0.25 mg cm^{-2} was loaded.

4.6 Bulk CO_2 electrolysis and product analysis. 1-hr bulk CO_2 electrolysis experiments were performed using a custom-built H-cell (Pine Research) coupled with an online microGC for gaseous product detection. Using a PMC-500/LO Potentiostat (Princeton Applied Research), the chronoamperometry experiments were performed by holding the potential at values between -0.6 and -1.2 V vs. RHE. For all experiments, the working, reference and counter electrodes were a fresh sheet of the silver nanoparticle catalyst (~ 1 cm^2), Ag|AgCl (Pine Research) and a 3 mm diameter graphite rod (Sigma Aldrich), respectively. The two halves of the H-cell were separated by a Nafion 115 membrane (Fuel Cell Store). The working half-cell was sealed so that it was gas tight and contained 30 mL of the CO_2 purged electrolyte, the working electrode and the reference electrode. Bulk CO_2 electrolysis was carried out in 5 different electrolytes: 0.1 molal. $KHCO_3$, 8 wt.% PEI, 10 wt.% NOHM-I-PEI, 8 wt.% HPE and 10 wt.% NOHM-I-HPE, where all polymer and NOHM-based electrolytes were doped with 0.1 molal. $KHCO_3$. In every experiment, the counter half-cell contained 30 mL of CO_2 purged 0.1 molal $KHCO_3$ and the counter electrode. The counter half-cell was left open to the atmosphere to prevent any pressure buildup within the H-cell. Prior to starting the 1-hr chronoamperometry experiments, the silver nanoparticle catalysts were cleaned using a cyclic volatammetry sweep program and the resistance of the solution was compensated for using an iR detection function on the potentiostat.

The gas phase products (*i.e.,* H_2 and CO) were analyzed using a previously calibrated microGC Fusion Analyzer (Inficon) during the course of the reaction. A constant stream of CO_2 (45-50 mlpm) flowed through the working half-cell and passed through a gas dryer before arriving at the microGC, where a custom program was developed for the online collection, with sampling occurring every ~5 minutes. A schematic of our setup for the online CO_2RR product measurement is displayed in **Figure S6**. The main species detected were H_2, CO and CO_2, with trace amounts of N_2 and O_2 observed as well. Using the properties of the gases and the measured flowrate, the detected volume concentrations of H_2 and CO were converted to mole concentrations and then integrated with respect to time to determine the total number of moles of each product collected over the course of each 1-hr electrolysis experiment. The Faradaic efficiency (FE) was calculated using the following equation

$$FE(\%) = \frac{nFmol_i}{C} \times 100\% \qquad \textbf{Eq. (14)}$$

where n is the number of electrons transferred per mole of product (n = 2 for both H_2 and CO formation), F is Faraday's constant (96,485 C/mol electron), mol_i refers to the total moles of compound i formed at time, t, and C is the total charge transferred at time, t.

4.7 Imaging and elemental mapping of the Ag nanoparticle electrodes. To visualize the effect of PEI, NOHM-I-PEI, HPE and NOHM-I-HPE addition on the CO_2RR and to confirm the presence of polymers/NOHMs on the electrode surface, SEM imaging and elemental mapping were performed. The electrode was analyzed using a scanning electron microscope with 5 and 10 kV (Zeiss Sigma VP SEM) equipped with energy-dispersive spectroscopy (EDS), 10 kV, (Bruker XFlash 6| 30 EDS). The electrodes were characterized after being held at -1.2 V vs. RHE for 1 hr in each of the 5 CO_2 purged electrolytes studied: 0.1 molal. $KHCO_3$, 8 wt.% PEI, 10 wt.% NOHM-I-PEI, 8 wt.% HPE and 10 wt.% NOHM-I-HPE. All polymer and NOHM-based electrolytes were doped with 0.1 molal. $KHCO_3$. Before imaging the electrodes, they were rinsed with DI water immediately after the reaction was completed and then dried overnight under vacuum at 25 °C to remove any residual moisture.

Acknowledgements

This work was funded by Shell's Long Range Research and Experimentation (LRRE) Program. We would also like to acknowledge LRRE's Dense Energy Carriers team (DEC) for their useful input and discussions during the course of this work. Additionally, the authors would like to acknowledge Breakthrough Electrolytes for Energy Storage (BEES), an Energy Frontier Research Center funded by the U.S. Department of Energy, Office of Science, Basic Energy Sciences under Award # DE-SC0019409 for funding the part of the work focused on exploring the catalyst-electrolyte interactions (SEM-EDS imaging).

References

[1] S. R. Sinsel, R. L. Riemke, V. H. Hoffmann, *Renew. Energy* **2020**, *145*, 2271.

[2] G. Glenk, S. Reichelstein, *Nat. Energy* **2019**, *4*, 216.

[3] W. Ren, C. Zhao, **2019**, 2019.

[4] Y. Y. Birdja, E. Pérez-gallent, M. C. Figueiredo, A. J. Göttle, F. Calle-vallejo, M. T. M. Koper, *Nat. Energy* **2019**, *4*.

[5] M. B. Ross, P. De Luna, Y. Li, C. Dinh, D. Kim, P. Yang, E. H. Sargent, *Nat. Catal.* **2019**, *2*.

[6] D. T. Whipple, P. J. A. Kenis, *J. Phys. Chem. Lett.* **2010**, *1*, 3451.

[7] T. Ping, Y. Dong, S. Shen, *ACS Sustain. Chem. Eng.* **2020**, *8*, 18071.

[8] B. Qin, Y. Li, H. Fu, H. Wang, S. Chen, Z. Liu, F. Peng, *ACS Appl. Mater. Interfaces* **2018**, *10*, 20530.

[9] Z. Liang, L. Song, M. Sun, B. Huang, Y. Du, *Sci. Adv.* **2021**, *7*, 1.

[10] S. Cui, C. Yu, X. Tan, H. Huang, X. Yao, J. Qiu, *ACS Sustain. Chem. Eng.* **2020**, *8*, 3328.

[11] S. A. Ghoneim, R. A. El-Salamony, S. A. El-Temtamy, *World J. Eng. Technol.* **2016**, *04*, 116.

[12] Q. Lu, F. Jiao, **2016**, *29*, 439.

[13] N. Han, P. Ding, L. He, Y. Li, Y. Li, **2020**, *1902338*, 1.

[14] L. Fan, C. Xia, F. Yang, J. Wang, H. Wang, Y. Lu, **2020**, 1.

[15] S. Malkhandi, B. S. Yeo, *Curr. Opin. Chem. Eng.* **2019**, *26*, 112.

[16] S. Liang, N. Altaf, L. Huang, Y. Gao, Q. Wang, *J. CO2 Util.* **2020**, *35*, 90.

[17] M. Konig, J. Vaes, E. Klemm, D. Pant, *iScience* **2019**, *19*, 135.

[18] S. Sharifi Golru, E. J. Biddinger, *Chem. Eng. J.* **2022**, *428*, 131303.

[19] B. Kim, J. Choi, H. Kim, **2018**.

[20] B. A. Rosen, J. L. Haan, P. Mukherjee, B. Braunschweig, W. Zhu, A. Salehi-Khojin, D. D. Dlott, R. I. Masel, *J. Phys. Chem. C* **2012**, *116*, 15307.

[21] B. A. Rosen, I. Hod, **2018**, *1706238*, 1.

[22] C. V. Amanchukwu, *Joule* **2020**, *4*, 281.

[23] M. Moura, D. S. Pupo, R. Kortlever, **2019**, 2926.

[24] I. Sullivan, A. Goryachev, I. A. Digdaya, X. Li, H. A. Atwater, D. A. Vermaas, C. Xiang, *Nat. Catal.* **2021**, *4*, 952.

[25] L. Sun, G. K. Ramesha, P. V. Kamat, J. F. Brennecke, *Langmuir* **2014**, *30*, 6302.

[26] B. A. Rosen, A. Salehi-Khojin, M. R. Thorson, W. Zhu, D. T. Whipple, P. J. A. Kenis, R. I. Masel, *Science (80-.).* **2011**, *334*, 643.

[27] Z. P. Jovanov, J. F. De Araujo, S. Li, P. Strasser, **2019**.

[28] L. Chen, F. Li, Y. Zhang, C. L. Bentley, M. Horne, A. M. Bond, J. Zhang, *ChemSusChem* **2017**, *10*, 4109.

[29] F. Quan, M. Xiong, F. Jia, L. Zhang, *Appl. Surf. Sci.* **2017**, *399*, 48.

[30] S. Garg, M. Li, T. E. Rufford, L. Ge, V. Rudolph, R. Knibbe, **2020**, 304.

[31] D. V Vasilyev, A. V Rudnev, P. Broekmann, P. J. Dyson, **2019**, 1635.

[32] S. Verma, X. Lu, S. Ma, R. I. Masel, P. J. A. Kenis, *Phys. Chem. Chem. Phys.* **2016**, *18*, 7075.

[33] N. Ahmad, X. Wang, P. Sun, Y. Chen, F. Rehman, J. Xu, X. Xu, *Renew. Energy* **2021**, *177*, 23.

[34] M. Abdinejad, Z. Mirza, X. Zhang, H. Kraatz, **2020**.

[35] E. Pérez-Gallent, C. Vankani, C. Sánchez-Martínez, A. Anastasopol, E. Goetheer, *Ind. Eng. Chem. Res.* **2021**, *60*, 4269.

[36] G. Lee, Y. C. Li, J. Y. Kim, T. Peng, D. H. Nam, A. Sedighian Rasouli, F. Li, M. Luo, A. H. Ip, Y. C. Joo, E. H. Sargent, *Nat. Energy* **2021**, *6*, 46.

[37] Y. Cui, B. He, X. Liu, J. Sun, *Ind. Eng. Chem. Res.* **2020**, *59*, 20235.

[38] B. A. Rosen, A. Salehi-Khojin, M. R. Thorson, W. Zhu, D. T. Whipple, P. J. A. Kenis, R. I. Masel, *Science (80-.).* **2011**, *334*, 643.

[39] M. Asadi, K. Kim, C. Liu, A. V. Addepalli, P. Abbasi, P. Yasaei, P. Phillips, A. Behranginia, J. M. Cerrato, R. Haasch, P. Zapol, B. Kumar, R. F. Klie, J. Abiade, L. A. Curtiss, A. Salehi-Khojin, *Science (80-.).* **2016**, *353*, 467.

[40] A. Ati, D. W. Boyce, J. L. Dimeglio, J. Rosenthal, **2018**.

[41] W. Ren, X. Tan, X. Chen, G. Zhang, K. Zhao, W. Yang, C. Jia, Y. Zhao, S. C. Smith, C. Zhao, *ACS Catal.* **2020**, *10*, 13171.

[42] H. K. Lim, H. Kim, *Molecules* **2017**, *22*, 536.

[43] B. Ratschmeier, B. Braunschweig, *J. Phys. Chem. C* **2021**, *125*, 16498.

[44] L. Sun, G. K. Ramesha, P. V. Kamat, J. F. Brennecke, *Langmuir* **2014**, *30*, 6302.

[45] K.-Y. A. Lin, A.-H. A. Park, *Environ. Sci. Technol.* **2011**, *45*, 6633.

[46] C. Petit, S. Bhatnagar, A.-H. A. Park, *J. Colloid Interface Sci.* **2013**, *407*, 102.

[47] K.-Y. A. Lin, C. Petit, A.-H. A. Park, *Energy & Fuels* **2013**, *27*, 4167.

[48] T. G. Feric, S. T. Hamilton, A. Haque, J. Jeddi, J. Sangoro, M. D. Dadmun, A.-H. A. Park, *Adv. Funct. Mater.* **2022**, *2203947*, 1.

[49] K.-Y. A. Lin, Y. Park, C. Petit, A.-H. A. Park, *RSC Adv.* **2014**, *4*, 65195.

[50] C. Petit, K.-Y. A. Lin, A.-H. A. Park, *Langmuir* **2013**, *29*, 12234.

[51] T. G. Feric, S. T. Hamilton, A. H. A. Park, *Energy and Fuels* **2021**, *35*, 19592.

[52] G. Rim, T. G. Feric, T. Moore, A.-H. A. Park, *Adv. Funct. Mater.* **2021**, *31*, 1.

[53] N. M. Cantillo, M. Bruce, S. T. Hamilton, T. G. Feric, A.-H. A. Park, T. Zawodzinski, *J. Electrochem. Soc.* **2020**, *167*, 116508.

[54] J. L. Schaefer, S. S. Moganty, D. A. Yanga, L. A. Archer, *J. Mater. Chem.* **2011**, *21*, 10094.

[55] S. Srivastava, S. Choudhury, A. Agrawal, L. A. Archer, *Curr. Opin. Chem. Eng.* **2017**, *16*, 92.

[56] Y. Park, K.-Y. A. Lin, A.-H. A. Park, C. Petit, *Front. Energy Res.* **2015**, *3*, 1.

[57] Y. Park, J. Decatur, K.-Y. A. Lin, A.-H. A. Park, *Phys. Chem. Chem. Phys.* **2011**, *13*, 18115.

[58] S. Choi, S. Moon, Y. Park, *Langmuir* **2020**, *36*, 9626.

[59] C. Petit, Y. Park, K.-Y. A. Lin, A.-H. A. Park, *J. Phys. Chem. C* **2012**, *116*, 516.

[60] Y. Park, C. Petit, P. Han, A.-H. A. Park, *RSC Adv.* **2014**, *4*, 8723.

[61] Y. Park, D. Shin, Y. N. Jang, A.-H. A. Park, *J. Chem. Eng. Data* **2012**, *57*, 40.

[62] S. Overa, T. G. Feric, A.-H. A. Park, F. Jiao, *Joule* **2021**, *5*, 8.

[63] A. Agrawal, S. Choudhury, L. A. Archer, *RSC Adv.* **2015**, *5*, 20800.

[64] S. Choudhury, A. Agrawal, S. Wei, E. Jeng, L. A. Archer, *Chem. Mater.* **2016**, *28*, 2147.

[65] M. D. Tikekar, L. A. Archer, D. L. Koch, *J. Electrochem. Soc.* **2014**, *161*, A847.

[66] S. T. Hamilton, T. G. Feric, G. Andrzej, N. M. Cantillo, T. A. Zawodzinski, A. A. Park, *ACS Appl. Mater. Interfaces* **2022**, *14*, 22016.

[67] Y. Zhang, D. Poe, L. Heroux, H. Squire, B. W. Doherty, Z. Long, M. Dadmun, B. Gurkan, M. E. Tuckerman, E. J. Maginn, *J. Phys. Chem. B* **2020**, *124*, 5251.

[68] J. M. Klein, H. Squire, W. Dean, B. E. Gurkan, *J. Phys. Chem. B* **2020**, *124*, 6348.

[69] N. K. Jayakody, C. C. Fraenza, S. G. Greenbaum, D. Ashby, B. S. Dunn, *J. Phys. Chem. B* **2020**, *124*, 6843.

[70] S. Liu, M. Walton, N. V. Tarakina, P. Akcora, *J. Phys. Chem. B* **2020**, *124*, 4843.

[71] M. D. Dadmun, M. A. Haque, T. G. Feric, S. T. Hamilton, A.-H. A. Park, *J. Phys. Chem. C* **2021**, *125*, 5327.

[72] J. M. Klein, H. Squire, B. Gurkan, *J. Phys. Chem. C* **2020**, *124*, 5613.

[73] E. U. Mapesa, N. M. Cantillo, S. T. Hamilton, M. A. Harris, T. A. Zawodzinski, A. A. Park, J. Sangoro, *Macromolecules* **2021**, *54*, 2296.

[74] T. G. Feric, S. T. Hamilton, N. M. Cantillo, A. E. Imel, T. A. Zawodzinski, A.-H. A. Park, *J. Phys. Chem. B* **2021**, *125*, 9223.

[75] S. T. Hamilton, T. G. Feric, S. Bhattacharyya, N. M. Cantillo, S. G. Greenbaum, T. A. Zawodzinski, A.-H. A. Park, *J. Am. Chem. Soc. Au* **2022**.

[76] W. Yu, T. Wang, A.-H. A. Park, M. Fang, *Nanoscale* **2019**, *11*, 17137.

[77] S. Liguori, J. Wilcox, *Curr. Trends Futur. Dev. Membr. Carbon Dioxide Sep. by Using Membr.* **2018**, 385.

[78] X. Wang, C. Song, *Front. Energy Res.* **2020**, *8*.

[79] R. R. Bhosale, A. Kumar, F. Almomani, U. Ghosh, A. Alnouss, J. Scheffe, R. B. Gupta, *Ind. Eng. Chem. Res.* **2016**, *55*, 5238.

[80] H. M. Stowe, G. S. Hwang, *Ind. Eng. Chem. Res.* **2017**, *56*, 6887.

[81] B. Lv, B. Guo, Z. Zhou, G. Jing, *Environ. Sci. Technol.* **2015**, *49*, 10728.

[82] S. Zhang, Y. Shen, P. Shao, J. Chen, L. Wang, *Environ. Sci. Technol.* **2018**, *52*, 3660.

[83] E. F. Da Silva, H. F. Svendsen, *Ind. Eng. Chem. Res.* **2004**, *43*, 3413.

[84] H. Guo, C. Li, X. Shi, H. Li, S. Shen, *Appl. Energy* **2019**, *239*, 725.

[85] D. Filotás, T. Nagy, L. Nagy, P. Mizsey, G. Nagy, *Electroanalysis* **2018**, *30*, 690.

[86] C. Delacourt, P. L. Ridgway, J. B. Kerr, J. Newman, *J. Electrochem. Soc.* **2007**.

[87] M. R. Singh, E. L. Clark, A. T. Bell, *Phys. Chem. Chem. Phys.* **2015**, *17*, 18924.

[88] M. Dunwell, Q. Lu, J. M. Heyes, J. Rosen, J. G. Chen, Y. Yan, F. Jiao, B. Xu, *J. Am. Chem. Soc.* **2017**, *139*, 3774.

[89] A. S. Varela, M. Kroschel, T. Reier, P. Strasser, *Catal. Today* **2016**, *260*, 8.

[90] P. Bumroongsakulsawat, G. H. Kelsall, *Electrochim. Acta* **2014**, *141*, 216.

[91] M. R. Singh, Y. Kwon, Y. Lum, J. W. Ager, A. T. Bell, *J. Am. Chem. Soc.* **2016**, *138*, 13006.

[92] L. Q. Zhou, C. Ling, M. Jones, H. Jia, *Chem. Commun.* **2015**, *51*, 17704.

[93] E. L. Clark, S. Ringe, M. Tang, A. Walton, C. Hahn, T. F. Jaramillo, K. Chan, A. T. Bell, **2019**.

[94] M. Bhattacharya, S. Sebghati, Y. M. Vercella, C. T. Saouma, *J. Electrochem. Soc.* **2020**, *167*, 086507.

[95] K.-Y. A. Lin, C. Petit, A.-H. A. Park, *Energy & Fuels* **2013**, *27*, 4167.

[96] Y. Park, D. Shin, Y. N. Jang, A.-H. A. H. A. Park, *J. Chem. Eng. Data* **2012**, *57*, 40.

[97] S. Moon, Y. Lee, S. Choi, S. Hong, S. Lee, A.-H. A. Park, Y. Park, *Org. Process Res. Dev.* **2018**, *22*, 1723.

[98] B. H. Ko, B. Hasa, H. Shin, E. Jeng, S. Overa, W. Chen, F. Jiao, *Nat. Commun.* **2020**, *11*, 1.

NOHMs (Nanoparticle Organic Hybrid Materials) consist of a polymer canopy tethered to a nanoparticle core and have been proposed for combined CO_2 capture and electrochemical conversion. The ionic conductivity and CO_2 binding energy of the polymer canopy (*i.e.,* chemisorption vs. physisorption) were identified as critical design parameters that could enable the production of highly tunable syngas compositions over a silver nanoparticle catalyst in CO_2 electroreduction.

Tony G. Feric, Sara T. Hamilton, Byung H. Ko, Ga-Hyun A. Lee, Sumit Verma, Feng Jiao and Ah-Hyung Alissa Park

Highly Tunable Syngas Product Ratios Enabled by Novel Nanoscale Hybrid Electrolytes Designed for Combined CO_2 Capture and Electrochemical Conversion